International Journal of Neural Systems, Vol. 30, No. 7 (2020) 2050018 (15 pages)

DOI: 10.1142/S0129065720500185

World Scientific
www.worldscientific.com

A Prototype of EEG System for IoT

Francisco Laport, Adriana Dapena*, Paula M. Castro,
Francisco J. Vazquez-Araujo and Daniel Iglesia
Department of Computer Engineering
CITIC Research Center & University of A Coruña
Campus de Elviña, A Coruña 15071, Spain
**adriana.dapena@udc.es*

Accepted 5 February 2020
Published Online 4 May 2020

In this work, we develop open source hardware and software for eye state classification and integrate it with a protocol for the Internet of Things (IoT). We design and build the hardware using a reduced number of components and with a very low-cost. Moreover, we propose a method for the detection of open eyes (oE) and closed eyes (cE) states based on computing a power ratio between different frequency bands of the acquired signal. We compare several real- and complex-valued transformations combined with two decision strategies: a threshold-based method and a linear discriminant analysis. Simulation results show both classifier accuracies and their corresponding system delays.

Keywords: Electroencephalography; Internet of Things; prototype; signal processing.

1. Introduction

Brain–Computer Interfaces (BCI) are communication systems that monitor the cerebral activity and translate certain characteristics, corresponding to user intentions, to commands for device control.[1] One of the greatest challenges of BCI technology is the development of wearable and portable electrode devices that are minimally invasive and ready-to-use with short training times.[2,3] In particular, current research is focused on the potential of Electroencephalography (EEG)[4–6] techniques to capture the brain activity associated to user intent.[7–9] This requires the design and development of friendly devices with real-time operation and adaptation for people with motor functional diversity. Recently, different companies and studies have presented commercial products with the aim of opening the EEG technology to applications not restricted to medical diagnosis,[2,10] such as the Emotiv Epoc[11] and the NeuroSky Mindwave.[12] However, both the Emotiv or NeuroSky devices require the use of accompanying proprietary software.

In this work, we present a prototype of an EEG device designed to acquire signals using a reduced number of sensors. The system is composed of low-cost components, including a dual core microcontroller that allows us to perform all operations associated to signal classification simultaneously to the transmission of data to the Internet of Things (IoT) environment. Our first objective is the assessment of its performance in determining the user's eye states, i.e, open eyes (oE) or closed eyes (cE), using different strategies based on short training times. These strategies are as follows:

(1) Real-valued instead of complex-valued transforms, since, in general, the use of complex-valued signals requires more than twice the number of computational operations.

*Corresponding author.

(2) Sliding windows with overlapping instead of the traditional approach based on nonoverlapped windows, thus reducing delays between acquisition and decision.
(3) A classifier based either on a threshold-based method or on Linear Discriminant Analysis (LDA).
(4) A correction system for the mitigation of decision errors.

Our second objective is the use of the acquired information about the user's eye state for the control of IoT devices by means of ON/OFF operations.

This paper is organized as follows. Section 2 summarizes some of the most important previous works related to the utilization of EEG for IoT and to the classification of cE and oE states from acquired signals. Section 3 describes our open source device for EEG signal acquisition and an open solution from OpenBCI.[13] Section 4 shows the architecture used to integrate the EEG device with IoT elements. Section 5 explains the proposed method for cE and oE classification. The methodology and materials used for the experiments are presented in Sec. 6. Section 7 shows the results obtained from a set of test individuals. Section 8 analyzes these results. Finally, Sec. 9 contains the more relevant conclusions of this work.

2. Related Work

The IoT paradigm refers to a global dynamic infrastructure based on interoperable communication protocols that integrate physical and virtual objects into an information network.[14] Among other applications, home automation or smart homes are rapidly gaining interest.[15,16] The aim of such systems is to make the home environment not only comfortable and accessible, but also to optimize and automate the use of appliances like TV sets, air conditioners, light bulbs, ovens or washing machines.

The development of low-cost EEG devices as a tool for IoT has been presented in some recent papers.[17] For instance, Jadadish *et al.* present a BCI application which detects voluntary blinks of the user and controls electrical appliances included in an IoT system. Mathe *et al.*[18] connect a BCI application which employs the Mindwave[12] consumer EEG device to estimate the user's depression level with an IoT ecosystem responsible for notifying the caretakers. In a more recent study with the same headset, Narayana *et al.*[19] present a BCI running on an Android phone which locks/unlocks a wheelchair and controls its movements through an IoT environment. Lee *et al.*[20] present a BCI-controlled mobile robot for telepresence which is developed in an IoT system and used for the communication between subject and robot.

In previous work, we have studied the control of IoT devices using the detection of cE and oE states.[21] For the detection of each state, we analyzed the alpha and beta waves of the EEG signal. Alpha waves, whose frequency ranges from 8 Hz to 13 Hz, are associated with the most relaxed and stable brain state; whereas beta waves, in the frequency range from 13 Hz to 22 Hz, are associated with states of high wakefulness.[22–25]

Both the eye state identification and the eye-gaze analysis have become an active research field during the last years due to their implication in human–machine interfaces.[26,27] In particular, EEG eye state detection has been successfully applied in a wide variety of domains,[28] such as driving drowsiness detection,[29] infant sleep-waking state classification[30] and stress features identification,[31] among others. Several papers have associated cE and oE with particular frequency and amplitude ranges of the brain waves.[22–25] For instance, Kirkup *et al.*[32] present a home automation control system for a rapid on/off switch appliance which filters the EEG signal between 8 Hz and 12 Hz and employs the resulting alpha values to determine the user's eye state based on a threshold.

In a more recent study, Saghafi *et al.* propose the use of delta and theta bands for these purposes, applying an 8 Hz low-pass filter to the EEG signal[33] and using different methods for the extraction of the principal features in eye state classifiers such as, for example, Multivariate Empirical Mode Decomposition (MEMD), Logistic Regression (LR), Artificial Neural Networks (ANN) or Support Vector Machine (SVM). Their proposed algorithm detected the eye state with an accuracy of 88.2% in less than 2 s.

On the other hand, Naderi *et al.*[34] propose a technique based on Welch's method for estimating the Power Spectral Density (PSD) and on Recurrent Neural Networks (RNNs) to differentiate a relaxed and open eye state from an epileptic seizure. Features

from EEG time series and PSD levels were extracted to train and test the classifier which, at the end, exhibited an accuracy of 100%. In another study on the same dataset, Acharya *et al.*[35] propose the use of Convolutional Neural Networks (CNN) for the development of a Computer-Aided-Diagnosis (CAD) system that automatically detects seizure using EEG signals. They implement an algorithm based on a 13-layer deep convolutional neural network for the detection of normal, preictal, and seizure classes, where the normal state corresponds to a relaxed and CE situation. Their proposed technique achieves an accuracy, specificity, and sensitivity of 88.67%, 90.00%, and 95.00%, respectively. Wang *et al.*[28] extracted channel standard deviations and averages as features for an Incremental Attribute Learning (IAL) algorithm and achieved an error rate of 27.45% for eye state classification.

Although the aforementioned papers show methods to detect eye states with high accuracy, they gather the brain activity using at least 14 electrodes and large EGG devices. The main drawback of these devices is that they are uncomfortable for the user and cumbersome to use for long periods of time and during daily life activities. Moreover, they use large training sequences. In order to avoid these limitations, we have proposed a simple threshold-based algorithm that uses the power of both alpha and beta bands with short training periods.[21] Following this idea, this paper studies the employment of different criteria to detect changes on the eye states.

3. Open Devices

The elements of the EEG device we developed are shown in Fig. 1. This prototype has a total of three sensors: input, reference and ground.

The input signal is amplified and bandpass filtered between 4.7–29.2 Hz. We use an AD8221 instrumentation amplifier followed by: (i) a 50 Hz notch filter to avoid the interference of electric devices in the vicinity of the sensor wires; (ii) a second-order low-pass filter; (iii) a second-order high-pass filter; and (iv) a final bandpass filter with adjustable gain. The different filter stages that follow the instrumentation amplifier are shown in Fig. 2. Both the low and high-pass filters use a Sallen–Key architecture.[36] The low-pass filter has a cut-off frequency of

$$f_{c1} = \frac{1}{2\pi \cdot 300 \times 10^3 \cdot 10 \times 10^{-9} \cdot \sqrt{3.3}} = 29.204\,\text{Hz},$$

and a Q-factor of

$$Q = \frac{\sqrt{3.3}}{2} = 0.908,$$

whereas the high-pass filter has a cut-off frequency of

$$f_{c2} = \frac{1}{2\pi \cdot 470 \times 10^{-9} \cdot 100 \times 10^3 \cdot \sqrt{1.961}} = 4.742\,\text{Hz},$$

and a Q-factor of

$$Q = \frac{\sqrt{1.961}}{2} = 0.7.$$

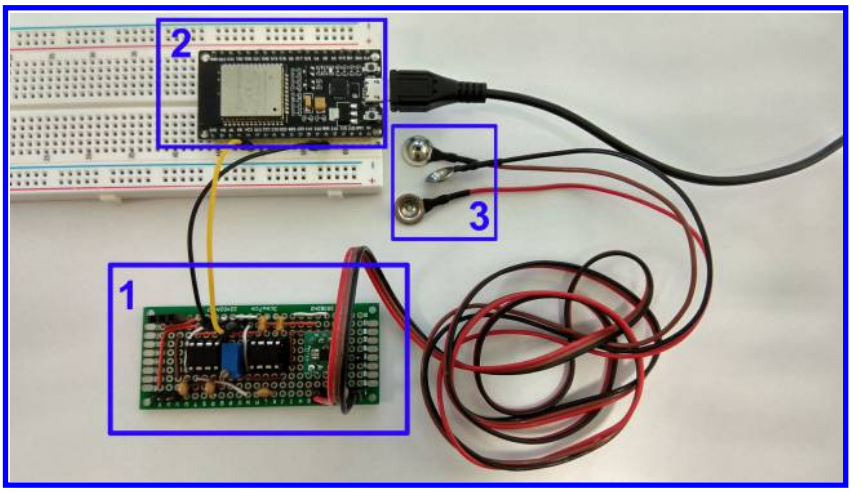

Fig. 1. Proposed device details. (1) Amplifier; (2) ESP32 module and (3) Sensors.

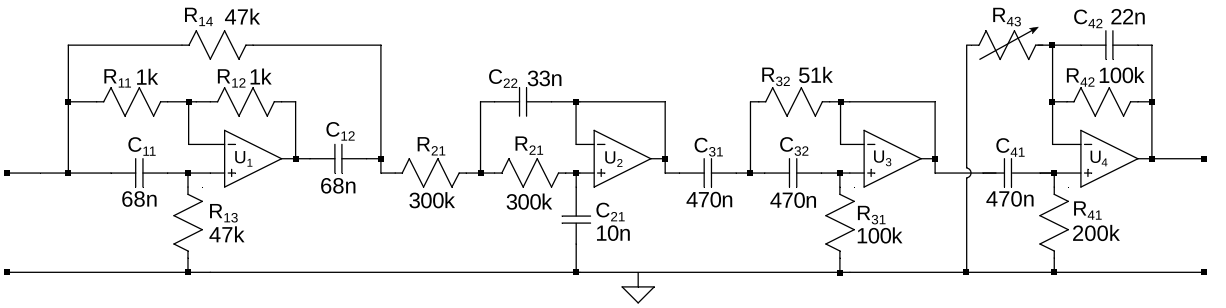

Fig. 2. EEG sensor filters.

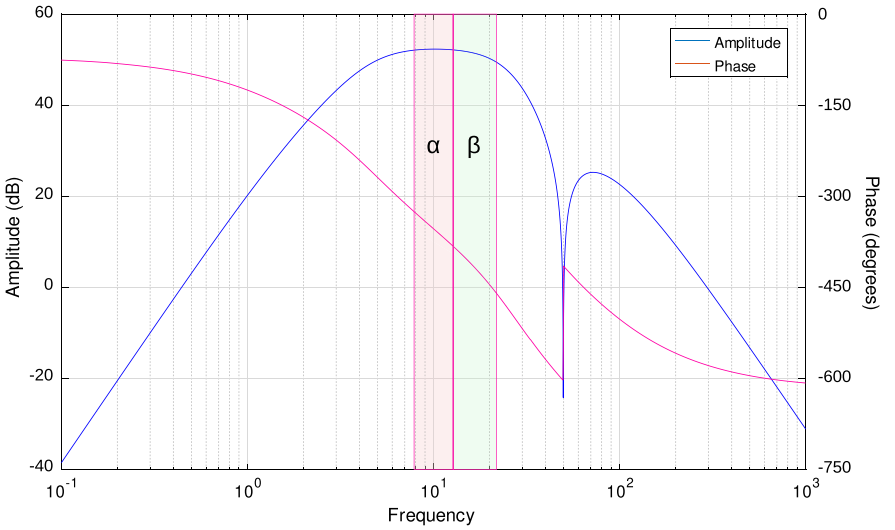

Fig. 3. EEG filter response.

The Q-factor of the high-pass filter is higher in order to compensate the response of the notch filter near the 30 Hz cut-off frequency. The final bandpass filter has cut-off frequencies of

$$f_{c3l} = \frac{1}{2\pi \cdot 470 \times 10^{-9} \cdot 200 \times 10^{3}} = 1.693\,\text{Hz},$$

and

$$f_{c3h} = \frac{1}{2\pi \cdot 22 \times 10^{-9} \cdot 100 \times 10^{3.}} = 72.343\,\text{Hz},$$

and a gain of

$$G = 1 + \frac{100 \times 10^{3}}{R_{43}}.$$

The R_{43} potentiometer, with values up to 1 kΩ, allows us to adjust the gain to better utilize the whole range of the ADC.

Figure 3 shows the response of the filter stages for $R_{43} = 220\,\Omega$, which results in a gain of 53.171 dB.

Table 1. Basic comparison of EEG devices.

Device	Cyton	Prototype
Available channels	8	1
Used channels	1	1
Sampling rate (Hz)	250	200
Wet/dry electrodes	Wet	Wet
ADC resolution	24 bits	12 bits
Wireless transmission	BLE	Wi-Fi
Signal extraction	EEG, EMG & ECG	EEG

Table 1 summarizes some of the specifications of the proposed device and compares it with the well-known hardware: the OpenBCI Cyton board.[13] OpenBCI is built around an ADS1299, developed by Texas Instruments for biopotential measurements. The ADS1299 is an 8-channel, low-noise, 24-bit analog-to-digital converter specifically designed for

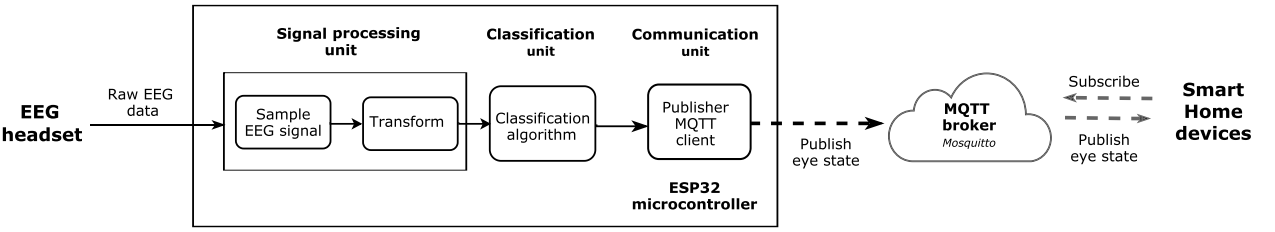

Fig. 4. Proposed system architecture.

measuring EEG signals. The OpenBCI uses an ATmega328P microcontroller and a SD card for local storage. EEG signals are sampled at 250 Hz. Data acquired from this device is bandpass filtered between 3 and 45 Hz. An adjustable 50 Hz or 60 Hz notch filter can also be applied.

4. System Design and Architecture

Figure 4 shows the architecture for the integration of our BCI device in an IoT environment. The aim of the system is to detect cE or oE and employ this information in the control of different surrounding devices. The IoT ecosystem is composed of the EEG device described in Sec. 3 and its BCI application, together with other household devices whose behavior depends on the produced information.

The communication between the different IoT agents is based on the Message Queue Telemetry Transport (MQTT) protocol.[37] It is a publish/subscribe, extremely simple and lightweight messaging protocol designed for constrained devices and low-bandwidth networks. The publish/subscribe model is built around a central broker and a number of clients which connect to the broker. Publishers send messages to the broker on a specific topic and subscribers register with the broker their interest in one or more of them. The broker acts like an intermediary agent, responsible for relating the information that the publishers provide with the subscriber clients and dealing with authentication and controlling who is allowed to publish or subscribe to which topics. The topics can be created and combined in a simple way, so the system can be easily expanded with the inclusion of new devices or applications into the new topics.

For the architecture shown in Fig. 4, the BCI application, running on the ESP32, is the first publisher client of the IoT ecosystem. It is in charge of detecting the eye state of the user and, making use of the built-in Wi-Fi module, publishing the extracted information to the broker. The MQTT broker deals with the messages received from the BCI application and forwards it to interested subscribers. The transmitted data correspond to one byte of information, which represents the ocular state of the user. The broker is deployed in a Raspberry Pi 2 model B and implemented using Eclipse Mosquitto,[38] an open source and lightweight MQTT broker.

The data transmission in the MQTT protocol is performed through the exchange of a series of MQTT Control Packets (CP). These CP consist of up to three parts: (1) a fixed header, which is always present in all CP; (2) an optional variable header and (3) an optional payload. This final part of the CP is used by the application to publish the information extracted by the system. The protocol allows CP sizes up to 256 MB.[39]

A wide variety of household devices can be included in the system as subscriber clients (e.g. light bulbs, kitchen burners, heating system). These devices receive the information from the broker and react accordingly to it, e.g. if the kitchen burners client observes that the user has had their eyes closed for a long time, which likely means that he or she has fallen asleep, then the subscriber client should turn the burners off in order to avoid any risk.

5. Proposed Threshold-Based Classifier

Power Spectral Density Analysis (PSDA), which is based on the frequency analysis of the EEG signal, is one of the most widely used feature extraction methods for EEG classification. The PSD represents the distribution of signal power in different bands. In particular, we will use the power ratio between alpha and beta frequency bands for the determination of the user's eye state. In this section, we will introduce different transforms and the method to detect cE and oE.

5.1. *Sliding transforms*

Let $x(n)$ be the sample at the discrete instant n of the zero-mean signal x. The Sliding Transform (ST) is obtained by applying an N-point discrete transform to moving windows starting at instant n_r i.e. $\{x(n_r), x(n_r+1), \ldots, x(n_r+N-1)\}$. The signal in the transform-domain is given by the following expression:

$$X(\omega_k, n_r) = \sum_{n=0}^{N-1} x(n_r+n)\cdot\phi(w_k, n), \quad k = 0, \ldots, N-1, \tag{1}$$

where ϕ is, in general, a complex-valued function and w_k denotes the frequency bin. Note that this expression corresponds to the DFT when ϕ is

$$\phi_1(\omega_k, n) = e^{j\omega_k n} = \cos(\omega_k n) + j\sin(\omega_k n), \tag{2}$$

where $\omega_k = \frac{2\pi k}{N}$.

We will also consider the complex-valued function expressed as

$$\phi_2(\omega_k, n) = \text{sign}(\cos(\omega_k n)) + j\,\text{sign}(\sin(\omega_k n)). \tag{3}$$

Two additional real-valued functions are also considered in this work, given by

$$\phi_3(\omega_k, n) = \cos(\omega_k n), \tag{4}$$

$$\phi_4(\omega_k, n) = \text{sign}(\cos(\omega_k n)), \tag{5}$$

respectively denoted as ϕ_3 and ϕ_4 transforms.

All the aforementioned transforms are directly computed in the EPS32 presented in Fig. 1. Note that the ϕ_2 transform only takes values $\pm 1 \pm j$ and therefore, the products in (2) can be easily implemented at low-level by only two sign changes per $x(n_r+n)$ sample. Contrary to the ϕ_1 and ϕ_2 transforms, both ϕ_3 and ϕ_4 only use the real part of the DFT and, as a consequence, the number of operations is also reduced in half with respect to the two first transforms. Moreover, since the ϕ_4 transform only takes values $+1$ and -1, only one sign change per $x(n_r+n)$ sample is computed in (2).

In this work, we propose to compute the transforms described above on overlapped sliding windows. In general, we need to compute (2) over the input windows beginning at instant n_r, without taking into account the result obtained for previous windows. However, for some transforms, the computational overhead can be considerably reduced by using recursive algorithms.[40,41]

5.2. *Decision algorithm*

Using (2), we can compute the alpha and beta bands taking into account that the alpha band ranges from 8 Hz to 13 Hz, while the beta band ranges from 14 Hz to 19 Hz. From each band, we obtain the power of alpha and beta, respectively denoted by α and β, and calculate their ratio $R = \beta/\alpha$. Note that R is a real number for all real- or complex-valued transforms. Taking advantage of the ratio fluctuation according to the eye state, a threshold-based classifier is implemented for the detection of cE or oE user states. Those values that fall below that threshold, termed as T, will be classified as cE, while those above it will be associated to oE. Thus, the criteria for our classifier is defined by the following decision rule:

$$\begin{aligned} &\text{cE}, \quad R \le T, \\ &\text{oE}, \quad R > T. \end{aligned} \tag{6}$$

The threshold value is determined in a training step by computing the power of alpha and beta bands and then the $R = \beta/\alpha$ ratio for cE and oE sates, respectively denoted by R_{cE} and R_{oE}. Subsequently, we have obtained that threshold applying the following expression:

$$T = \frac{\max(R_{\text{cE}}) + \min(R_{\text{oE}})}{2}. \tag{7}$$

To improve the robustness of the threshold calibration, we compute the ratio R for each window of the training set. Then, all the values that lie more than three standard deviations away from the mean are treated as outliers and are not taken into account for the calculation of T in (7).

In order to test the performance of our proposed classifier, we will compare it with Linear Discriminant Analysis (LDA). The basis of LDA is the use of hyperplanes that separate the feature vectors of the different classes.[42,43] The location and orientation of these hyperplanes is determined from training data. LDA has lower computational requirements and faster rates than other popular classifiers such as Support Vector Machine (SVM) or Radial Basis Function (RBF), which makes it suitable for the development of online BCI systems.[6] Moreover, LDA is probably the most used classifier for BCI design.[44]

5.3. *Stability strategy*

The criteria in (6) takes a decision each time a window is processed without taking into account the previous state. Since our architecture uses that information to send an order to the IoT device, an erroneous decision implies a nonstable system.

To mitigate sudden changes in the environment caused by artifacts or abnormal EEG data, we propose to use the criteria (6) as a tentative for cE or oE state decision. If this tentative results in a change of the user's eye state, the classifier waits for the result from the next window before taking a decision. If the next window results in the same message of state change, the classifier decides that the change has indeed ocurred. Otherwise, the tentative decision is discarded.

6. Materials and Methods

The participant group included a total of seven volunteers (males) who agreed to participate in the research. Their mean age was 29.67 (range 24–56). The participants indicated that they do not have hearing or visual impairments. Participation was voluntary and informed consent was obtained for each participant in order to employ their EEG data in our study.

We captured the brain activity of the subjects with the proposed EEG prototype. Gold cup electrodes were placed in accordance with the 10–20 international system for electrode placement[45] and attached to the subjects scalp using a conductive paste. Electrode-skin impedances were checked to be below 15 kΩ at all electrodes. Several studies have proved that the alpha rhythm predominates in the occipital area of the brain when subjects remain with their eyes closed and it is reduced when visual stimulation takes place.[23,46,47] In accordance with these works, the input channel of the prototype was located in the O2 position. Moreover, to reduce the setup time and improve the EEG signal quality, the reference and ground electrodes were placed in the FP2 and A1 positions, respectively, where the absence of hair facilitates its placement[48] (see Fig. 5).

All the experiments were conducted in a sound-attenuated and controlled environment. Participants were seated in a comfortable chair and asked to be relaxed and focused on the task, trying to avoid any distraction or external stimulus. Experiments were

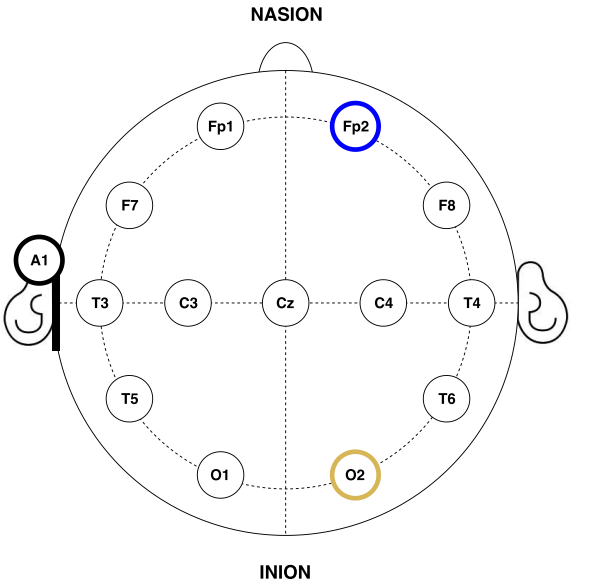

Fig. 5. Anatomical electrode distribution in accordance with the standard 10–20 placement system used during the EEG measurements. The yellow circle represents the input channel, while blue and black bordered circles represent reference and ground, respectively.

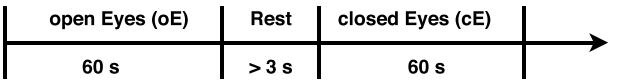

Fig. 6. User's experiment flowchart.

composed of 2 tasks: the first one, 60 s of oE and the second, 60 s of cE. Each task was separated by a pause of at least 3 s to ensure the participant is rested before a new task (see Fig. 6). In order to simulate a real-life situation, the subject could move his gaze freely during the eye-open tasks, without the need to keep it at a fixed point. The procedure was conveniently explained in advance allowing the participants to feel comfortable and familiar with the test environment. Possible artifacts were minimized by asking them not to speak, move or blink (or at least as little as possible) throughout the oE task.

A total of 10 tasks (i.e. 10 min) were recorded for each participant, which corresponds to five tasks of oE and five tasks of cE.

Since an essential feature of our proposed architecture is its ease of use and the users' comfort, a main objective of this system is to guarantee that the prototype achieves good performances using short training periods. For the developed experiments, the system was trained using 4 min of recorded data,

where 2 min correspond to the oE state, and the remaining 2 min to cE. From these data, the R ratio is calculated for each window considering each type of transform. These ratios are then used to calibrate the threshold level using (7) or to train the LDA classifier.

To compare the accuracies obtained using overlapped and nonoverlapped windows, several independent experiments were performed in which only the recordings not considered for the training step were used as test data, i.e. 3 min of data corresponding to each eye state. We have considered time windows of D seconds and an overlapped time slot of d seconds. Two important parameters must be considered for the design of these experiments:

- Computational overhead, which is given by the window size D that determines the number of samples used to compute transforms, denoted by N. Additionally, the number of windows grows with the size of the overlapped time slot i.e. d.
- Decision delay, which is the wait time for a new classifier decision, given by $D - d$ seconds.

The performance of each transform has been measured considering only the nonoverlapping samples, i.e. only the new instances, which correspond to the $D - d$ part of the window, are classified and taken into account for the calculation of the accuracy.

With the goal of avoiding classification bias each experiment has been repeated five times, each one implementing a hold out cross-validation process, i.e. random training and test recordings. Therefore, the results shown throughout this work correspond to the average of all of them.

7. Experimental Results

In this section we show the results obtained from experiments performed using the strategies proposed in Sec. 5. Additionally, we also include those achieved by the OpenBCI device for comparison.

7.1. *Threshold-based method*

Figure 7 shows the mean threshold obtained for each subject using nonoverlapped windows and different window sizes for the four transforms explained in

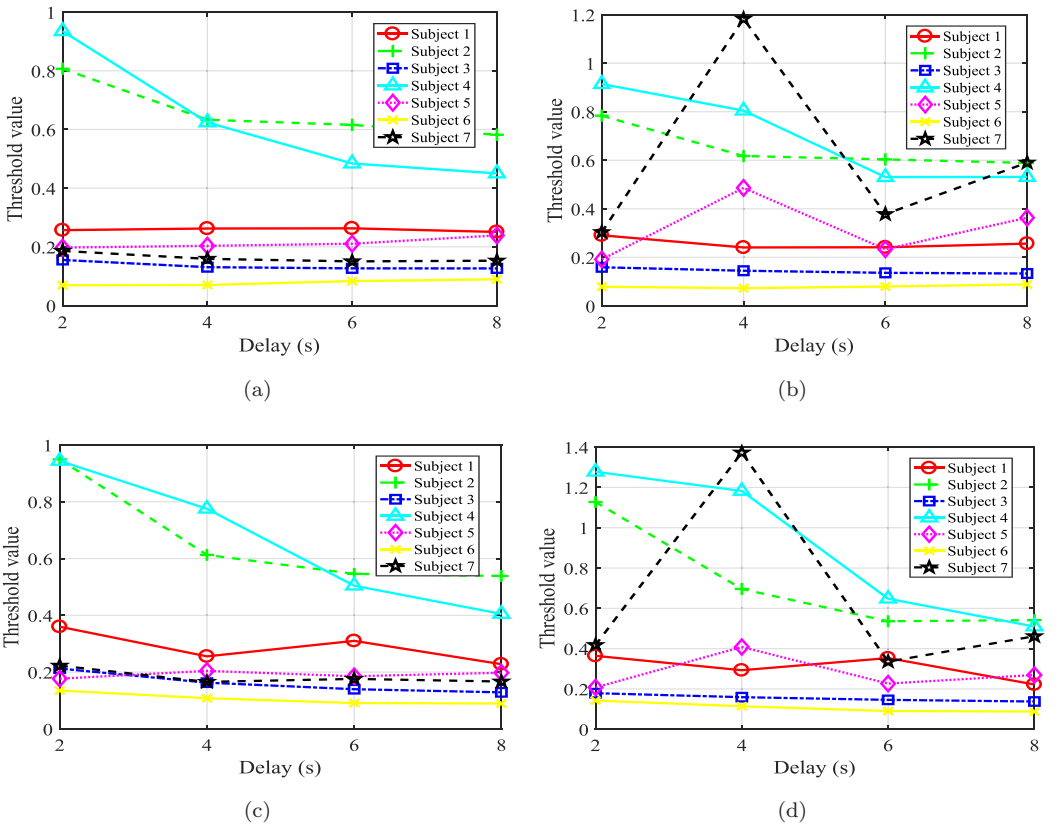

Fig. 7. Obtained users' threshold for the proposed transforms: (a) ϕ_1, (b) ϕ_2, (c) ϕ_3 and (d) ϕ_4.

Sec. 5.1. We can observe similarities between thresholds obtained for the ϕ_1 and ϕ_3 transforms, and also between those resulted from the ϕ_2 and ϕ_4 transforms.

First, we present results corresponding to experiments performed using nonoverlapped windows. In this case, the decision delay is the same as the window size, i.e. $D - d = D$ seconds. Table 2 shows the results obtained from recordings of both oE and cE states. We can observe that the system presents good results for cE (above 85% for all cases), especially for the ϕ_1 transform, and higher as the decision delay is less restricted. Conversely, the system performance for oE shows lower accuracies, where delays of 6 s or 8 s are needed to achieve higher than 85%.

For the second experiment, we consider overlapped windows of size $D = 10$ s and different overlapped sizes i.e. d is variable. Table 3 shows the results obtained from oE and cE recordings. We can observe that all the accuracies have considerably improved for short delays compared to nonoverlapped windows (see Table 2). In particular, the ϕ_1 transform achieves an accuracy above 93% for both eye states and all the delays.

We now evaluate the behavior of our system for oE and cE detection on each subject. We use window sizes of $D = 10$ s. Figures 8(a) and 8(b) show the accuracies and standard deviations obtained from oE and cE recordings considering 2 s as decision delay. The equivalent results for a higher delay of 4 s are depicted in Figs. 8(c) and 8(d). It can be observed that the accuracies obtained for the classification of oE and ϕ_1 are greater than 90% for all the subjects, with Subject 7 achieving the lowest results with an accuracy of 92.22% and 93.78% for delays of 2 s and 4 s, respectively. For cE the best transform is also ϕ_1, although for one subject, denoted by 4, it shows worse performance with accuracies below 90% (specifically 86% and 84.89% for delays of 2 s and 4 s, respectively). This percentage implies that, in these cases, the devices connected an IoT environment may turn on/off needlessly.

Table 2. Performances for nonoverlapped windows with the threshold-based classifier.

	Delay $D - d$ (s)			
Transform	2	4	6	8
(a) Accuracy for oE				
ϕ_1	76.60	87.62	92.92	94.86
ϕ_2	74.98	86.73	89.87	94.35
ϕ_3	63.87	81.08	85.81	94.22
ϕ_4	60.73	77.33	86.13	93.59
(b) Accuracy for cE				
ϕ_1	86.41	89.68	92.95	93.81
ϕ_2	86.00	89.11	92.48	93.71
ϕ_3	86.41	87.24	88.98	89.87
ϕ_4	86.51	85.75	87.59	88.63

Table 3. Performances for overlapped windows with the threshold-based classifier.

	Delay $D - d$ (s)			
Transform	2	4	6	8
(a) Accuracy for oE				
ϕ_1	96.35	97.08	95.97	95.24
ϕ_2	94.06	94.86	92.73	93.21
ϕ_3	92.25	93.40	91.49	91.94
ϕ_4	90.89	90.79	88.98	90.38
(b) Accuracy for cE				
ϕ_1	95.27	94.83	94.35	93.94
ϕ_2	93.37	93.40	93.46	92.44
ϕ_3	92.13	92.44	91.40	92.13
ϕ_4	91.21	91.56	89.49	92.19

7.2. *LDA*

The previous experiments were also performed to test the performance of the LDA classifier. Tables 4 and 5 show the results obtained for cE and oE applying the four proposed transforms when the R ratio is extracted considering nonoverlapped or overlapped windows, respectively. It can be observed that for both cases, the oE performance is significantly lower than that achieved by the threshold-based method. For the ϕ_1 transform, the maximum accuracy for nonoverlapped windows is 86.10% with a delay of 8 s, whereas for overlapped windows the accuracy is 86.89% with a delay of 2 s.

Figure 9 shows the performance achieved by each subject with decision delays of 2 s and 4 s. It can be seen that 4 of the 7 subjects present an average accuracy below 90% for oE.

7.3. *Stability strategy*

Finally, we will consider the strategy explained in Sec. 5.3 in which the decision about a state change

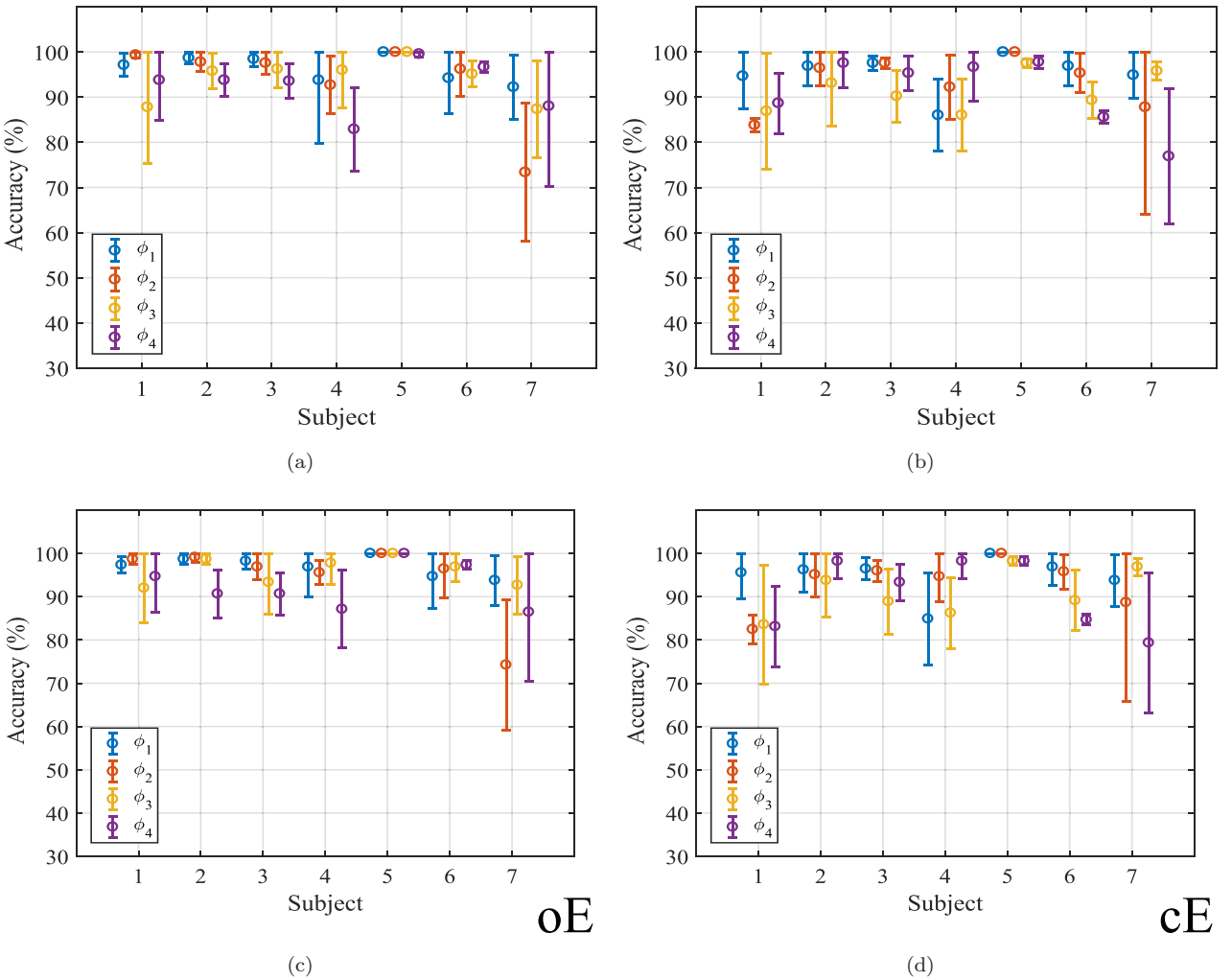

Fig. 8. Classification accuracies and standard deviation with the threshold-based method: (a) oE with decision delay of 2 s, (b) cE with decision delay of 2 s, (c) oE with decision delay of 4 s and (d) cE with decision delay of 4 s.

Table 4. Performances for nonoverlapped windows with LDA.

	Delay $D-d$ (s)			
Transform	2	4	6	8
(a) Accuracy for oE				
ϕ_1	68.76	77.62	81.49	86.10
ϕ_2	68.83	81.05	81.11	83.68
ϕ_3	59.11	70.70	73.81	79.33
ϕ_4	57.52	67.68	75.37	78.67
(b) Accuracy for cE				
ϕ_1	90.51	94.92	97.75	97.94
ϕ_2	89.37	94.38	97.24	98.25
ϕ_3	89.30	92.25	94.35	96.76
ϕ_4	88.38	91.56	93.68	97.11

Table 5. Performances with overlapped windows with LDA.

	Delay $D-d$ (s)			
Transform	2	4	6	8
(a) Accuracy for oE				
ϕ_1	86.89	87.65	87.02	86.83
ϕ_2	86.06	86.73	86.25	86.10
ϕ_3	83.90	84.57	83.87	83.94
ϕ_4	81.68	82.32	82.00	83.02
(b) Accuracy for cE				
ϕ_1	98.19	98.70	98.22	98.44
ϕ_2	97.84	98.22	97.59	97.78
ϕ_3	96.89	96.51	96.06	97.14
ϕ_4	95.97	95.78	96.22	96.54

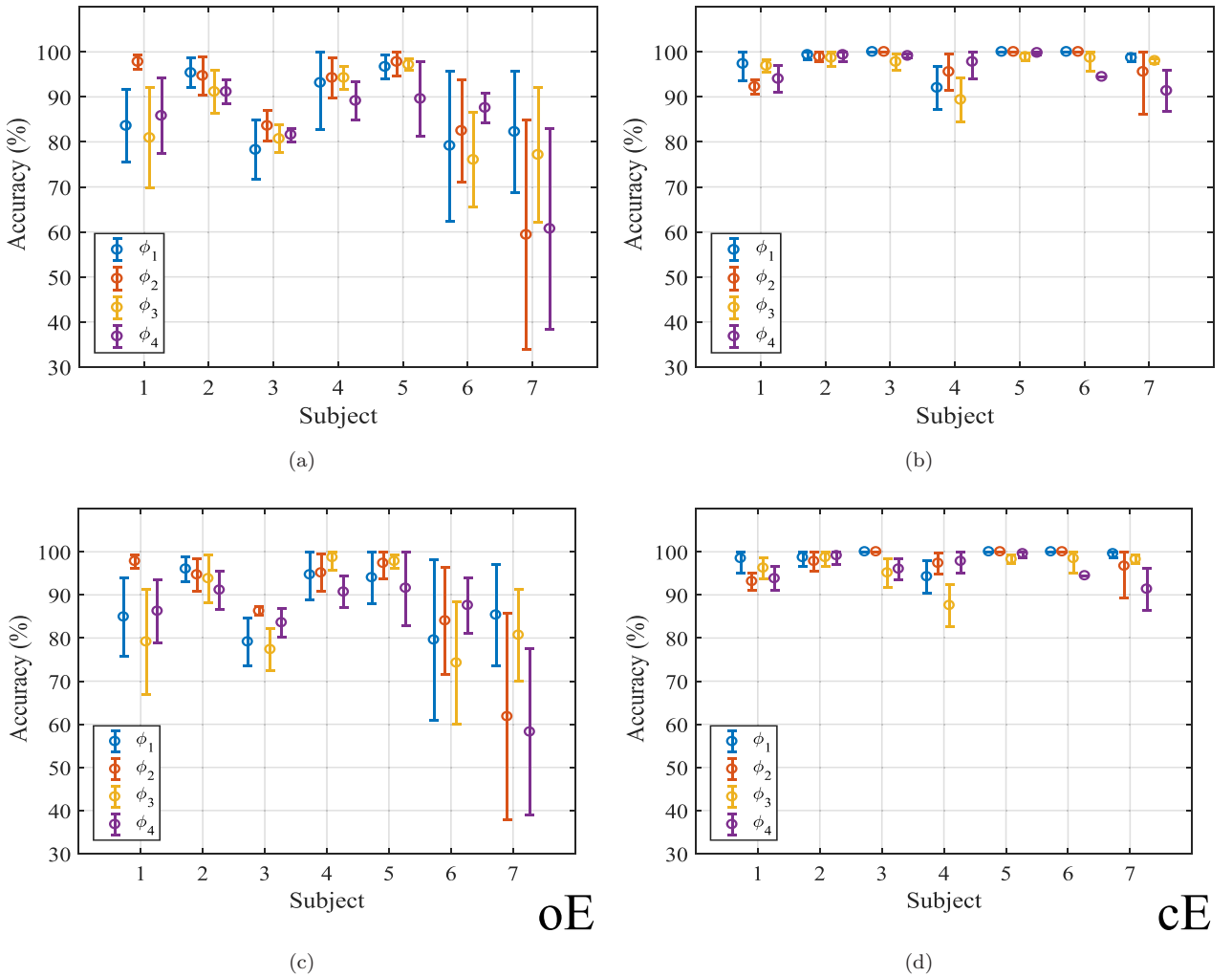

Fig. 9. Classification accuracies and standard deviation with Linear Discriminant Analysis: (a) oE with decision delay of 2 s, (b) cE with decision delay of 2 s, (c) oE with decision delay of 4 s and (d) cE with decision delay of 4 s.

is only executed if two consecutive windows agree. For this experiment, we will consider the ϕ_1 transform, which exhibited best performance before. It is important to note that this configuration has a delay of 2 s when the decision for the current window is the same as the previous one, and of 4 s otherwise.

We now consider EEG recordings registered by the proposed prototype and the Cyton board. Figure 10 compares both average accuracies and standard deviations of the classifiers. It can be observed that, in general, for the threshold-based method, both EEG devices achieve similar results, except for the subject 3 in oE and subject 4 in cE, where both devices differ notably. Moreover, it can be seen that this criteria is again significantly better for oE than LDA, although the accuracies are slightly lower for cE.

On the other hand, the results obtained for cE under this strategy outperform those corresponding to a delay of $D-d=2$ s depicted in Fig. 8(b) for the threshold criterion and in Fig. 9(b) for LDA.

7.4. *Data transmission*

As shown in Sec. 4, the ESP32 microcontroller performs the signal sampling. In this architecture, referred to as *Architecture* 1, the ESP32 also performs the state classification and the transmission of the results. An alternative architecture, termed as Architecture 2, consists on running the BCI

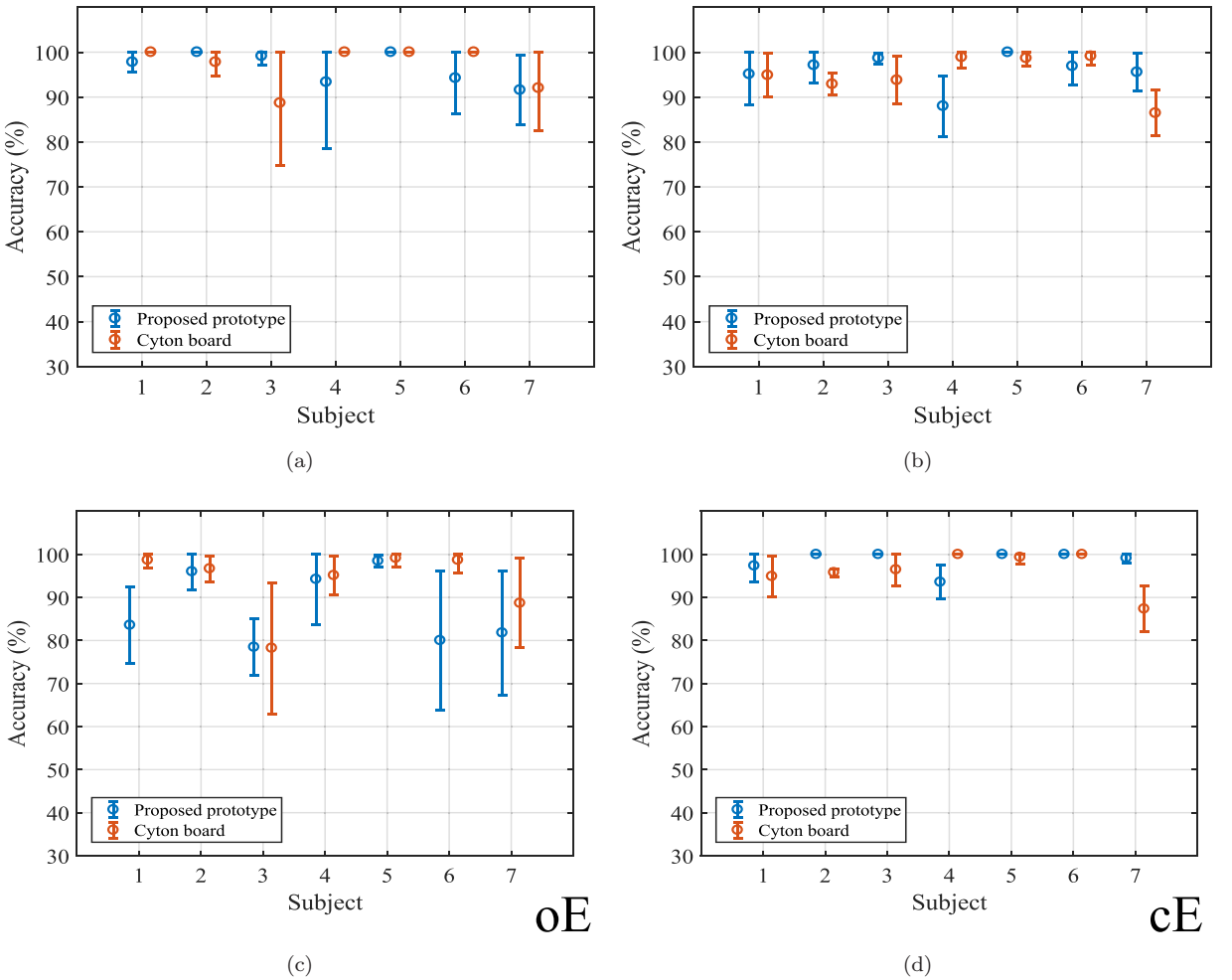

Fig. 10. Classification accuracies and standard deviation with the stability strategy and a final decision delay of 4 s: (a) oE for the threshold-based method, (b) cE for the threshold-based method, (c) oE for LDA and (d) cE for LDA.

Table 6. Payload size and number of packets sent during one minute for different architecture configurations.

Architecture	Method	Payload (bytes)	Packets
1	Eye state (2 s)	1	30
1	Eye state (4 s)	1	15
2	Samples	36,000	36,000
2	Samples (2 s)	1200	30
2	Samples (4 s)	2400	15

application in a control unit, like a Raspberry Pi or a PC. The ESP32 transmits samples directly to that control unit.

Table 6 shows the payload size and the number of packets sent during one minute for different architecture configurations. The first two rows show the data transmitted using Architecture 1 with delays of 2 s and 4 s. In this case, the payload of each packet will only contain one byte, which represents the user's eye state. The other three rows show the amount of data transmitted using Architecture 2, in which each packet contains the raw brain activity of the subject. For this purpose, two scenarios have been considered: first, the transmission of each sample captured by the EEG device, which allows the external devices to monitor the user's EEG data in real-time. Each sample is encoded in three bytes, so the system sends 36,000 bytes/minute for a sampling rate of 200 Hz. The second scenario corresponds to the transmission of chunks of recorded data corresponding to nonoverlapped slots (for delays of 2 s or 4 s).

8. Discussion

We have proposed an open EEG device that captures the brain activity of the subjects using only one input channel, located at position O2, in order to detect their eye state i.e. cE or oE. We have several requirements for the final system:

- The oE detection is usually more important to guarantee comfort.
- The accuracy must be high to avoid undesired situations in which devices turn off/on needlessly.
- Robustness against environment changes and the user's brain activity.
- Ready-to-use application, with short training times that facilitate its usability and integration in our daily life.

The system is trained using two minutes for each eye state and tested with three minutes per state. Tables 2–5 show the results obtained with both overlapped and nonoverlapped windows for the calculation of the R ratio. It is apparent that the use of overlapped windows significantly improves the system accuracy, especially for short delay times. Moreover, from the transform comparisons, we can conclude that all of them are adequate for cE detection. However, high accuracies for oE require a ϕ_1 transform computed from overlapped windows. For the shortest delays, the threshold-based classifier achieves an average accuracy of $95.81 \pm 3.67\%$, while LDA only obtains $92.54 \pm 8.19\%$.

From Figs. 8 and 9, we can observe that the threshold-based classifier performs notably better for the oE state than LDA, which achieves less than 90% of accuracy with the ϕ_1 transform for 4 out of 7 subjects and shows larger deviations. Conversely, the results obtained by LDA for cE show higher accuracies and shorter deviations than the threshold-based method, but these differences are much smaller than those of the oE experiments. Thus, the threshold-based classifier provides greater robustness for decision making, so it will be preferable for the implementation of the system. Note that the performance achieved by the ϕ_2 transform is slightly worse than that obtained by the ϕ_1 transform, although with a lower computational cost, as was mentioned before. Moreover, the success rates provided by the ϕ_3 and ϕ_4 transforms are not as high as for the first two transforms, but reduce the computational complexity even more.

Taking these results into account we can appreciate that, for a delay of 2 s, the threshold-based method obtains an accuracy greater than 90% for all the seven subjects in an oE scenario and for 6 of the 7 subjects for cE. This means that the system response time is suitable for the implementation of noncritical applications. However, for certain environments, this delay could produce user disagreements or possible artifacts and, therefore, should be reduced in future developments.

Moreover, Fig. 10 shows that the device proposed in this work achieves a performance that is at least similar to that of a widely-known commercial device such as the Cyton board. The stability strategy also presented here improves the accuracy achieved with most of the control subjects and reduces their deviation, thus providing a more robust operation with less false positive cases needlessly modifying the user's environment.

Future work includes adding more electrodes to the proposed prototype for the detection of signals from other brain areas, increasing the number of participants in the experiments and considering subjects with mobility disorders. Additionally, these experiments should be conducted in real scenarios to study their performance under real-life conditions.

9. Conclusions

The utilization of EEG for IoT is an emerging area. In this paper, we develop a low-cost open source EEG device which acquires EEG signals from one single channel. We use this prototype to determine the state of oE and cE. For this purpose, we propose a threshold-based algorithm that uses the ratio between the powers of the alpha and beta bands. We compare the performance obtained for different transforms applied on overlapping and nonoverlapping windows. The obtained results show the advantages of using overlapping windows to reduce decision delays and increase robustness. In this sense, we have reached high accuracies for both cE and oE detection independently from the employed transform, although for some subjects the discrete Fourier transform and its binary representation exhibit better results.

Acknowledgment

This work is the extension of the paper[21] published in the proceedings of the 8th International Work-Conference on the Interplay Between Natural and Artificial Computation (IWINAC 2019).[49,50]

Funding

This work has been funded by the Xunta de Galicia (ED431G2019/01), the Agencia Estatal de Investigación of Spain (TEC2016-75067-C4-1-R) and ERDF funds of the EU (AEI/FEDER, UE), and the predoctoral Grant No. ED481A-2018/156 (Francisco Laport). CITIC as a Research Centre of the Galician University System is financed by the Conselleria de Educacion, Universidades e Formacion Profesinal (Xunta de Galicia) through the ERDF (80%), Operational Programme ERDF Galicia 2014–2020 and the remaining 20% by the Secretaria Xeral de Universidades (Ref. ED431G 2019/01).

References

1. G. Pfurtscheller and C. Neuper, Motor imagery and direct brain-computer communication, *Proc. IEEE* **89**(7) (2001) 1123–1134.
2. A. Ortiz-Rosario and H. Adeli, Brain-computer interface technologies: From signal to action, *Rev. Neurosci.* **24**(5) (2013) 537–552.
3. A. Lécuyer, F. Lotte, R. B. Reilly, R. Leeb, M. Hirose and M. Slater, Brain-computer interfaces, virtual reality, and videogames, *Computer* **41**(10) (2008) 66–72.
4. S. Sanei and J. A. Chambers, *EEG Signal Processing* (John Wiley & Sons, 2013).
5. D. J. McFarland and J. R. Wolpaw, EEG-based brain-computer interfaces, *Current Opin. Biomed. Eng.* **4** (2017) 194–200.
6. A. Burns, H. Adeli and J. A. Buford, Brain–computer interface after nervous system injury, *Neurosci.* **20**(6) (2014) 639–651.
7. J. J. Vidal, Real-time detection of brain events, *Proc. IEEE* **65**(5) (1977) 633–641.
8. J. Wolpaw, N. Birbaumer, D. J. McFarland, G. Pfurtscheller and T. M. Vaughan, Brain-computer interfaces for communication and control, *Clin. Neurophysiol.* **113**(6) (2002) 767–791.
9. N. Elsayed, Z. S. Zaghloul and M. Bayoumi, Brain computer interface: EEG signal preprocessing issues and solutions, *Int. J. Comput. Appl.* **169**(3) (2017) 12–16.
10. C. T. Lin, L. W. Ko, M. H. Chang, J. R. Duann, J. Y. Chen, T. P. Su and T. P. Jung, Review of wireless and wearable electroencephalogram systems and brain-computer interfaces–a mini-review, *Gerontol.* **56**(1) (2010) 112–119.
11. *Emotiv. Brain Computer Interface Technology*, http://www.emotiv.com/.
12. *Neurosky*, http://www.neurosky.com/.
13. *OpenBCI*, http://openbci.com/.
14. A. Al-Fuqaha, M. Guizani, M. Mohammadi, M. Aledhari and M. Ayyash, Internet of things: A survey on enabling technologies, protocols, and applications, *IEEE Commun. Surv. Tutorials* **17** (2015) 2347–2376.
15. J. Gubbi, R. Buyya, S. Marusic and M. Palaniswami, Internet of things (iot): A vision, architectural elements, and future directions, *Future Gener. Comput. Syst.* **29**(7) (2013) 1645–1660.
16. D. Dietrich, D. Bruckner, G. Zucker and P. Palensky, Communication and computation in buildings: A short introduction and overview, *IEEE Trans. Ind. Electron.* **57** (2010) 3577–3584.
17. J. Minguillon, M. A. Lopez-Gordo, C. Morillas and F. Pelayo, A mobile brain-computer interface for clinical applications: From the lab to the ubiquity, *Biomedical Applications Based on Natural and Artificial Computing. IWINAC 2017.* Lecture Notes in Computer Science, Vol. 10338 (Springer, 2017), pp. 68–76.
18. E. Mathe and E. Spyrou, Connecting a consumer brain-computer interface to an internet-of-things ecosystem, in *Proc. 9th ACM Int. Conf. Pervasive Technologies Related to Assistive Environments*, Article No. 90 (2016) p. 2, https://doi.org/10.1145/2910674.2935844, doi:10.1145/2910674.2935844.
19. S. Narayana, R. V. Prasad and K. Warmerdam, Mind your thoughts: BCI using single EEG electrode, *IET Cyber-Phys. Syst. Theory & Appl.* **4**(2) (2018) 164–172.
20. R. Leeb, L. Tonin, M. Rohm, L. Desideri, T. Carlson and J. R. Millán, Towards independence: A BCI telepresence robot for people with severe motor disabilities, *Proc. IEEE* **103**(6) (2015) 969–982.
21. F. Laport, F. J. Vazquez-Araujo, P. M. Castro and A. Dapena, Hardware and software for integrating brain–computer interface with internet of things, *Understanding the Brain Function and Emotions. IWINAC 2019.* Lecture Notes in Computer Science, Vol. 11486 (Springer, 2019), pp. 22–31.
22. E. D. Adrian and B. H. C. Matthews, The berger rhythm: Potential changes from the occipital lobes in man, *Brain* **57**(4) (1934) 355–385.
23. R. J. Barry, A. R. Clarke, S. J. Johnstone, C. A. Magee and J. A. Rushby, EEG differences between eyes-closed and eyes-open resting conditions, *Clin. Neurophysiol.* **118**(12) (2007) 2765–2773.
24. T. Cao, F. Wan, C. M. Wong, J. N. da Cruz and Y. Hu, Objective evaluation of fatigue by EEG spectral analysis in steady-state visual evoked potential-based brain-computer interfaces, *BioMed. Eng. Online* **13** (2014) 28.

25. J. B. Barry and F. M. De Blasio, EEG differences between eyes-closed and eyes-open resting remain in healthy ageing, *Biol. Psychol.* **129** (2017) 293–304.
26. J. Ma, Y. Zhang, A. Cichocki and F. Matsuno, A novel EOG/EEG hybrid human–machine interface adopting eye movements and ERPs: Application to robot control, *IEEE Trans. Biomed. Eng.* **62**(3) (2015) 876–889.
27. T. K. Reddy and L. Behera, Online eye state recognition from EEG data using deep architectures, in *Proc. 2016 IEEE Int. Conf. Systems*, *Man*, *and Cybernetics* (*SMC*) (Budapest, 2016), pp. 712–717.
28. T. Wang, S. U. Guan, K. L. Man and T. O. Ting, Time series classification for EEG eye state identification based on incremental attribute learning, in *2014 Int. Symp. Computer*, *Consumer and Control* (*IS3C*) (Taichung, 2014), pp. 158–161.
29. M. V. M. Yeo, X. Li, K. Shen and E. P. V. Wilder-Smith, Can svm be used for automatic EEG detection of drowsiness during car driving? *Saf. Sci.* **47**(1) (2009) 115–124.
30. P. A. Estévez, C. M. Held, C. A. Holzmann, C. A. Perez, J. P. Pérez, J. Heiss, M. Garrido and P. Peirano, Polysomnographic pattern recognition for automated classification of sleep-waking states in infants, *Med. Biol. Eng. Comput.* **40**(1) (2002) 105–113.
31. N. Sulaiman, M. N. Taib, S. Lias, Z. H. Murat, S. A. M. Aris and N. H. A. Hamid, Novel methods for stress features identification using EEG signals, *Int. J. Simul. Syst. Sci. Technol.* **12**(1) (2011) 27–33.
32. L. Kirkup, A. Searle, A. Craig, P. McIsaac and P. Moses, EEG-based system for rapid on-off switching without prior learning, *Med. Biol. Eng. Comput.* **35**(5) (1997) 504–509.
33. A. Saghafi, C. P. Tsokos, M. Goudarzi and H. Farhidzadeh, Random eye state change detection in real-time using EEG signals, *Expert Syst. Appl.* **72**(1) (2017) 42–48.
34. M. A. Naderi and H. Mahdavi-Nasab, Analysis and classification of EEG signals using spectral analysis and recurrent neural networks, in *2010 17th Iranian Conf. Biomedical Engineering* (*ICBME*) (IEEE, 2010), pp. 1–4.
35. U. R. Acharya, S. L. Oh, Y. Hagiwara, J. H. Tan and H. Adeli, Deep convolutional neural network for the automated detection and diagnosis of seizure using EEG signals, *Comput. Biol. Med.* **100** (2018) 270–278.
36. R. P. Sallen and E. L. Key, A practical method of designing rc active filters, *IRE Trans. Circuit Theory* **2**(1) (1955) 74–85.
37. J. M. Robinson, J. G. Frey, A. J. Stanford-Clark, A. D. Reynolds and B. V. Bedi, Sensor networks and grid middleware for laboratory monitoring, *First Int. Conf. e-Science and Grid Computing*, 2005, pp. 562–569.
38. *Eclipse Mosquitto*, https://mosquitto.org/.
39. O. Standard, Mqtt version 3.1.1, http://docs. oasis-open, org/mqtt/mqtt/v3.1.1/mqtt-v3.1.1.html **1** (2014).
40. E. Jacobsen and R. Lyons, The sliding DFT, *IEEE Signal Process. Mag.* **20**(2) (2003) 74–80.
41. C. S. Park, Recursive algorithm for sliding walsh hadamard transform, *IEEE Trans. Signal Process.* **62**(11) (2014) 2827–2836.
42. K. Fukumug, *Statistical Pattern Recognition* (Academic Press, Inc, 1990).
43. R. O. Duda, P. E. Hart and D. G. Stork, *EEG Signal Processing* (Wiley Interscience, 2001).
44. F. Lotte, *Guide to Brain-Computer Music Interfacing* (Springer, 2014).
45. H. O. Klem, G. H. Luders, H. H. Jasper and E. C., The ten-twenty electrode system of the international federation, *Electroencephalograph. Clin. Neurophysiol. Suppl.* **52** (1958) 3–36.
46. D. La Rocca, P. Campisi and G. Scarano, EEG biometrics for individual recognition in resting state with closed eyes, in *2012 BIOSIG-Proc. Int. Conf. Biometrics Special Interest Group* (*BIOSIG*) (IEEE, 2012), pp. 1–12.
47. A. Gale, N. Dunkin and M. Coles, Variation in visual input and the occipital EEG, *Psychonomic Sci.* **14**(6) (1969) 262–263.
48. M. Ogino and Y. Mitsukura, Portable drowsiness detection through use of a prefrontal single-channel electroencephalogram, *Sensors* **18**(12) (2018) 4477.
49. J. M. F. de Vicente, J. R. Á. Sánchez, F. de la Paz López, F. J. Toledo-Moreo and H. Adeli (eds.), *Understanding the Brain Function and Emotions Proc. 8th Int. Work-Conference Interplay Between Natural and Artificial Computation* (*IWINAC 2019*), 3–7 June 2019, Almería, Spain, Part I Lecture Notes in Computer Science, Vol. 11486 (Springer, 2019), pp. 1–427.
50. J. M. F. de Vicente, J. R. Á. Sánchez, F. de la Paz López, F. J. Toledo-Moreo and H. Adeli (eds.), *From Bioinspired Systems and Biomedical Applications to Machine Learning Proc. 8th Int. Work-Conference Interplay Between Natural and Artificial Computation* (*IWINAC 2019*), *3–7 June 2019*, *Almería*, *Spain*, Part II Lecture Notes in Computer Science, Vol. 11487 (Springer, 2019), pp. 1–476.